Nanoscale elasticity measurement with in situ tip shape estimation in atomic force microscpoy

doi: 10.1063/1.1150627

Nanoscale elasticity measurement with *in situ* tip shape estimation in atomic force microscopy

Kazushi Yamanaka,[a] Toshihiro Tsuji, Atsushi Noguchi, Takayuki Koike, and Tsuyoshi Mihara
Department of Materials Processing, Tohoku University, Aoba02, Sendai 980-8579, Japan

(Received 1 October 1999; accepted for publication 2 March 2000)

For a quantitative evaluation of nanoscale elasticity, atomic force microscopy, and related methods measure the contact stiffness (or force gradient) between the tip and sample surface. In these methods the key parameter is the contact radius, since the contact stiffness is changed not only by the elasticity of the sample but also by the contact radius. However, the contact radius is very uncertain and it makes the precision of measurements questionable. In this work, we propose a novel *in situ* method to estimate the tip shape and the contact radius at the nanoscale contact of the tip and sample. Because the measured resonance frequency sometimes does not depend so sensitively on the contact force as expected from the parabolic tip model, we introduced a more general model of an axial symmetric body and derived an equation for the contact stiffness. Then, the parameters in the model are unambiguously determined from a contact force dependence of the cantilever resonance frequency. We verified that this method is able to provide an accurate prediction of the cantilever thickness, the tip shape, and the effective elasticity of soft and rigid samples. © *2000 American Institute of Physics.* [S0034-6748(00)05306-5]

I. INTRODUCTION

Quantitative measurement of nanoscale elasticity has increasingly become important for fundamental research of the physical properties of matter as well as quality control of modern micro- and nanoscale devices. Efforts for realizing this measurement applying atomic force microscopy (AFM) (Ref. 1) and near-field methods are reported. These include the scanning tunneling microscopy based method,[2] force modulation microscopy,[3,4] ultrasonic atomic force microscopy (UAFM),[5,6] and other higher-frequency vibration modes.[7–17] In these methods the measurable parameter is the contact stiffness,[18] or the ratio of contact force and the distance between the cantilever tip and sample surface. Through this parameter, images reflecting nanoscale elasticity of subsurface dislocations in graphite single crystal,[14–16] quantum dots,[17] and magnetic particles in storage media[12] were obtained.

At the same time, it is in principle possible to obtain quantitative values of elasticity using these methods, and some results are reported on gold[2] and polymer,[4,5] where comparison with the literature values was performed. However, no proof was presented for the obtained results. The major reason for the lack of proof is the lack of knowledge on the shape of the tip near the contact point, because the latter determines the radius of contact between the tip and sample. The change in contact radius tremendously changes the contact stiffness even if the elasticity of the sample is not changed.[18] Thus, the problem of tip shape attracted the attention of some previous authors,[22] but no attempt for a fundamental solution has been established. Therefore, the obtained results are not as reliable as in the elasticity measurements on the micrometer scale, known as acoustic microscopy,[19] where a precise calibration procedure is established.[20]

To solve this problem, we propose a novel *in situ* method for estimating the tip shape in this article, applicable to all methods in AFM and near-field mechanical probes. This method is based on a generalized theory of elastic contact for arbitrary axial symmetry tip[21,22,24] and an efficient inverse analysis procedure.[23] The information we use in the inverse analysis is the contact force dependence of the resonance frequency of cantilever deflection vibration. In Sec. II, we summarize the principle of UAFM that we use in this article for quantitative measurement. In Sec. III, we formulate the generalized theory of contact stiffness and discuss the condition where it is significantly different from the standard Hertzian contact mechanics.[18] Then, in Sec. IV, we obtain quantitative results for the inverse analysis and two proofs are presented to show that the estimated effective elasticity[18] is correct.

II. PRINCIPLE OF ULTRASONIC ATOMIC FORCE MICROSCOPY (UAFM)

The principle of UAFM (Ref. 5) is depicted in Fig. 1. We use this method because it has been proven to have the most advantageous property for quantitative analysis among AFM based methods,[24] although the approach proposed here is applicable to all other methods. Figure 1(a) shows a usual AFM. If the cantilever is soft enough, the tip does not deform the surface of stiff materials, such as hard polymers, metals, and ceramics. Thus, the topography of the sample surface can be precisely measured. However, the stiffness of the sample cannot be evaluated using the same cantilever,

[a]Author to whom correspondence should be addressed; electronic mail: yamanaka@material.tohoku.ac.jp

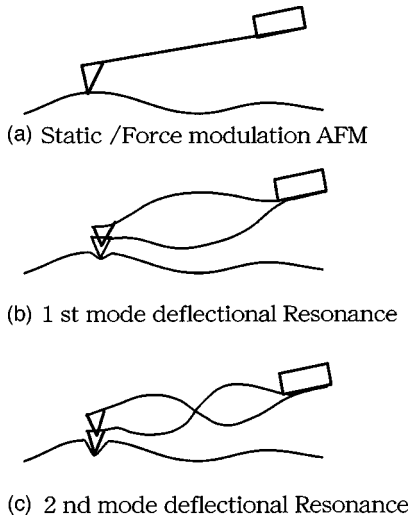

FIG. 1. Principle of ultrasoniic atomic force microscopy (UAFM).

since it is necessary to elastically deform the sample and measure the deformation for the elasticity measurement.

The UAFM is a novel method in AFM that eliminates the above dilemma using the mode dependent elastic behavior of a cantilever. As illustrated in Fig. 1(b), a resonant vibration is excited on the cantilever by applying a vibrating force to its base. Then, the sample is deformed according to the inertia force of the cantilever and tip, even if the stiffness of the cantilever is low. At the same time, the resonance frequencies as well as the vibration amplitude at fixed frequencies vary depending on the elasticity of the sample through the boundary condition at the tip–sample contact.[5] As a result, the elasticity of the sample can be evaluated by monitoring the cantilever vibration. When higher-order-mode vibration is excited, as shown in Fig. 1(c), the presence of nodes effectively enhances the cantilever stiffness, and the ability to deform the sample and evaluate the elasticity is enhanced. The advantage of UAFM over related techniques are the following.[5,24]

(1) High-resolution nanoscale spatial resolution is realized, which acoustic microscopes[19,20] cannot achieve.
(2) Nondestructive evaluation: the sample is not damaged. Recent technologies of nanoindentation can be applied to nanoscale resolution elasticity measurement,[25] but since the plastic deformation is induced on the sample, the elastic property is not necessarily identical to the intact surface.
(3) Quantitative evaluation: UAFM together with analyses given below provide the first quantitative elasticity evaluation in scanning probe microscopy.

Figure 2 shows an implementation of UAFM developed using a contact-mode AFM. In addition to the usual functions of AFM, a high-frequency vibrator attached to the support of a cantilever is driven by an output of a network analyzer (NWA). The resultant vibration of the cantilever is detected by a photodiode and processed by the NWA while the force is kept constant by the feedback loop of the *z* stage using the low-pass-filtered deflection signal (lower part of Fig. 2).

III. THEORY OF RESONANCE FREQUENCY AND CONTACT STIFFNESS

As shown previously, the resonance frequency of the UAFM cantilever is determined by the effective elasticity K (a function of Young's modulus and Poisson's ratio of the tip and sample) through the boundary condition at one end where the tip attached to the cantilever is in contact with the sample.[5] Recently, we found that careful measurements at low-excitation power, keeping the tip and sample in contact without jumping out, provide a resonance frequency compatible with the linear theory of cantilever vibration.[24]

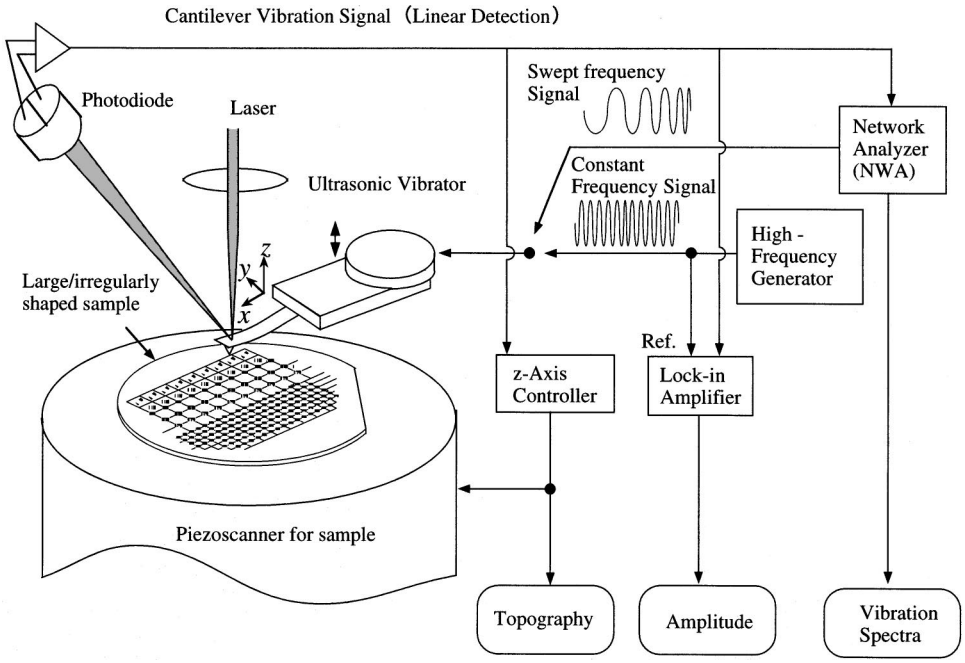

FIG. 2. Implementation of the UAFM system with a network analyzer. The high-frequency generator is used together with the lock-in amplifier to obtain amplitude images at a constant frequency. The network analyzer is used to obtain resonance frequencies and vibration spectra of the cantilever.

The resonance frequency is calculated from the frequency equation

$$\frac{k}{3S_V}(\kappa L)^3(1+\cos\kappa L\cosh\kappa L) = \cos\kappa L\sinh\kappa L-\sin\kappa L\cosh\kappa L, \quad (1)$$

where k is the cantilever stiffness, S_V is the (vertical) contact stiffness (slope of the force versus indentation depth relation), L is the cantilever length and $\kappa=(\omega^2\rho A/EI)^{1/4}$ is the wave number of the elastic wave on the cantilever in which ω is the angular frequency, ρ is the density, A is the area, E is the elastic modulus, and I is the moment of inertia of the cantilever, which depends on the width and the thickness of the cantilever. The cantilever stiffness k is given by $k=3EI/L^3$,[18] and in the case of rectangular section $k=Ewt^3/4L^3$, where w is the width and t is the thickness of cantilever. Though the nominal dimension of the cantilever is sometimes available, the value of thickness t is very often inaccurate. Therefore, we do not rely on the nominal value but estimate it for each cantilever.

The effect of lateral contact stiffness can be taken into account by modifying the boundary conditions. The resultant frequency equation is available in the literature.[10,11,24] Although this improvement is significantly important, especially at large normal force and for stiff materials, it is not used in this article. The possible error caused by the lateral force can to some extent be compensated by the calibration procedure shown below.

The contact stiffness in vertical direction S_V is usually approximated by the following equation:

$$S_V=(3/2)aK, \quad (2)$$

where a is the contact radius and $K=\frac{4}{3}[(1-\nu_{\mathrm{tip}}^2)/E_{\mathrm{tip}}+(1-\nu)^2/E]^{-1}$ is the effective elasticity.[18] The contact radius a increases with increasing force if the tip is sharp, whereas it remains constant if the tip is flat. Therefore, the sensitivity of the contact radius on the force depends on the bluntness of the tip. Usually, the tip shape is assumed to be parabolic and the Hertzian contact model[18] is used. However, we found that the tip is sometimes rather blunt, and the measured resonance frequency does not depend so sensitively on the contact force as expected from the parabolic tip model. Then, we introduce a more general model of an axial symmetric body.[21,22] Here, the profile of tip is expressed by an equation

$$Z=cr^n, \quad (3)$$

where z is the height and r is the radial distance of a point on the tip profile in the cylindrical coordinate, c is a constant and n is an arbitrary real number, which we call the tip shape index. For this tip profile, the approximation in Eq. (2) is not valid when the surface energy is dominant. Based on the theory of Maugis and Barquins,[21] we have derived an equation for the contact stiffness[24]

$$S_V=\frac{\partial F}{\partial\delta}=\frac{\partial F}{\partial a}\Big/\frac{\partial\delta}{\partial a} = \frac{\frac{3Kcn(n+1)}{2}\Psi a^n-\frac{3}{2}\sqrt{6\pi K\gamma a}}{(n+1)n\Psi ca^{n-1}-\frac{1}{2}\sqrt{\frac{8\pi\gamma}{3Ka}}}, \quad (4)$$

where γ is the surface energy change due to the increase of the unit contact area, and $\Psi=(\sqrt{\pi}/2)\Gamma(n/2+1)/\Gamma(n/2+3/2)$. It is easily seen that Eq. (4) is reduced to Eq. (2) when γ approaches zero, even when n is not equal to 2. However, since the surface energy becomes more dominant as the scale of contact is reduced, the use of Eq. (4) rather than Eq. (2) is essential in a the analysis of AFM (this is proven in Sec. IV).

In Eq. (4), the contact radius a is given by solving the equation

$$F=\frac{3Kcn}{2}\Psi a^{n+1}-\sqrt{6\pi K\gamma a^3}, \quad (5)$$

using the contact force F and the surface energy γ is determined from the measured pull of force F_c using the following equation:[22,24]

$$6\pi\gamma=\left[\frac{\left[\frac{2(n+1)}{2n-1}|F_c|\right]^{2n-1}[n(n+1)c\Psi]^3}{K^{n-2}}\right]^{1/(n+1)}. \quad (6)$$

In this formulation we have three unknown parameters, c, n, and t. To reduce the number of unknown parameters, the constant c in Eq. (3) is related to the tip shape index n using a measuring tip profile by a reference tip, a sharp needle of silicon crystal left in a porous silicon layer. If the origin of the measured profile is located at the apex of the tip and a reference point on the profile is given by (r_0,z_0), the constant c is related to the tip shape index n by

$$c=z_0r_0^{-n}. \quad (7)$$

IV. RESULTS AND DISCUSSION

As shown in the previous section, it is necessary for complete modeling of the operation of AFM to determine the tip shape index n, and another parameter, the cantilever thickness t. To achieve this, we use the shape of the force dependence of the resonance frequency. For the resonance frequency measurement, we used three sets of micromachined silicon cantilevers with a silicon tip. The nominal length, width, thickness, and stiffness of the cantilever were $L=444$ μm, $w=73$ μm, $t=3.5$ μm, and $k=1.5$ N/m, respectively. Another cantilever $L=226$ μm, $w=30.5$ μm, $t=3.0$ μm, and $k=3.0$ N/m, with a diamond-coated silicon tip, was also used. For the sample, four kind of materials, silicon crystal with a (100) surface, soda lime glass (GL), highly oriented pyrolytic graphite (GR), and polystyrene (PS), were used. The literature values of Young's modulus and Poisson's ratio (E,ν) used to calculate the effective elasticity K were (166 GPa, 0.22) for silicon, (62.0 GPa, 0.24)

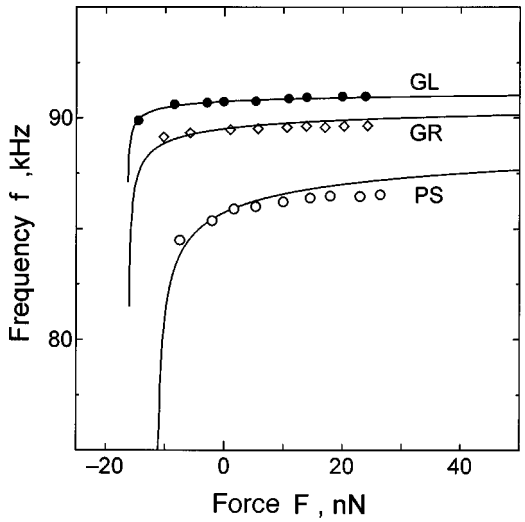

FIG. 3. Contact force dependence of the resonance frequency on soda lime glass (GL), highly oriented pyrolytic graphite (GR), and polystyrene (PS). The symbols are the measured resonance frequencies and the curves are the calculated ones based on the estimated tip shape index and cantilever thickness.

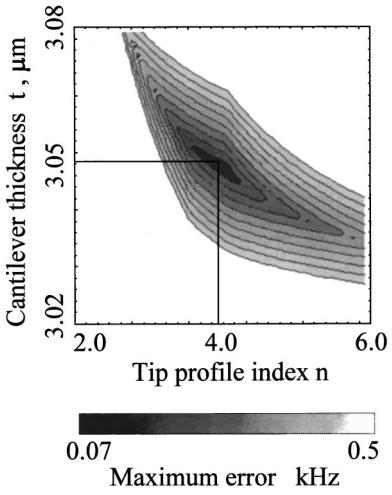

FIG. 4. Maximum error between measured and calculated resonance frequency as a function of cantilever thickness t and tip shape index n, based on the resonance frequencies in Fig. 3 for the soda lime glass (GL) using a silicon lever with a silicon tip.

for GL, (3.60 GPa, 0.35) for PS, and (30.0 GPa, 0.24) for GR. For silicon, the Voigt average[26] of the single-crystal elastic stiffness was employed. For graphite GR, the inverse of the compressibility in the direction of the c axis[27] was tentatively used for Young's modulus.

The closed circles in Fig. 3 are an example of the experimental force dependence of the resonance frequency obtained on a soda lime glass using a cantilever with a silicon tip. It is noted that the frequency was almost constant at large contact forces, but it decreased as the force decreased until the tip was pulled off the sample surface.

As the first step of analysis, we estimated the cantilever thickness and the tip shape index (t,n). To do this, we first assumed arbitrary initial values for the combination of (t,n). Then, we solved Eq. (5) for each contact force F to obtain the contact radius a. Next, we calculated the contact stiffness S_V using Eq. (4). Finally, we calculated the resonance frequency using Eq. (1). This calculation was repeated for the values of force where the resonance frequency was measured. Using these calculated resonance frequencies we evaluated the maximum difference between the measured and calculated resonance frequencies. Then, the maximum difference was minimized by appropriately changing the parameter set (t,n), using an efficient inverse analysis called the down-hill simplex method.[23] The inverse analysis searches for the minimum of the curved surface on (t,n) axes illustrated in Fig. 4. There is a sharp and unique minimum at $(t=0.34,\ n=5.6)$ in Fig. 4, and this minimum assures a satisfactory convergence of the inverse analysis. We repeated the same analyses for four different cantilevers.

As proof of the accuracy of the above analyses, we compared the estimated cantilever thickness t with the values measured in a scanning electron microscope (SEM). In the SEM observation, we found that the thickness was almost uniform along the cantilever, but has some variation, as shown by the horizontal error bars in Fig. 5. However, in all three cantilevers, good agreement was obtained between the estimated thickness and the average value of measured thickness. This result shows that the present model is applicable to the analysis in AFM. Although we used the model of the cantilever with a uniform rectangular cross section, a more accurate analysis taking into account the trapezoidal cross section gives even better results, as will be published later.

As another proof of the analysis, the profile of the tip was calculated based on Eq. (3) using the estimated tip shape index n, and compared with the measured profile. Then, we found that the estimated tip profile was very close to the

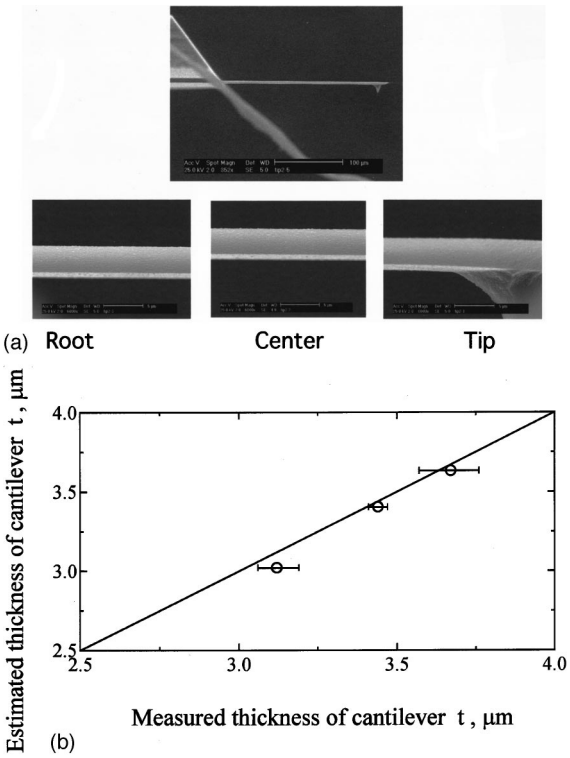

FIG. 5. Estimation accuracy of cantilever thickness. (a) Scanning electron microscope images of a cantilever. (b) Comparison between the estimated and measured thickness of the cantilevers showing remarkable agreement.

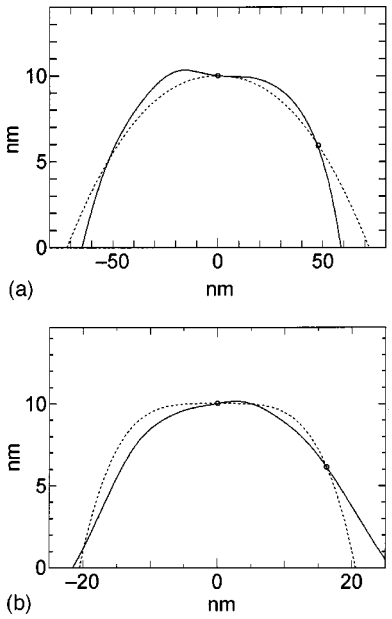

FIG. 6. Comparison between the estimated and measured tip profile. The solid curves represent the measured ones and the dotted curves represent the estimated ones. The circles show the origin and the reference point [see Eq. (7)] on the tip profile. (a) The tip used to obtain data in Fig. 3. The estimated profile is close to the measured one. (b) Another tip, where the estimated profile is more flat than the measured one.

measured one, as shown in Fig. 6(a). This result suggests a reasonable accuracy of the present analysis. It is important to note that the estimated tip shape index $n=5.6$ was significantly larger than 2 (for the parabolic tip model). This n indicates a flat shape and explains the slow increase of the resonance frequency as a function of force in Fig. 3. The usually assumed parabolic tip model gives a faster increase of the resonance frequency as the force is increased, because the contact radius is easily increased by increasing the force. Then, it cannot explain the observed flat force dependence.

Once the parameter set (t,n) is estimated, the contact stiffness of the unknown sample can be evaluated using the same parameter set. In this case, the unknown parameter is the effective elasticity K. Open squares and circles in Fig. 3 show the measured force dependence of the resonance frequencies on graphite and on polystyrene, respectively. The solid curves represent fitted curves using the same parameter set (t,n) obtained on GL, with the effective elasticity K adjusted so as to minimize the maximum error. The agreement between the measured and calculated force dependence of the resonance frequency is fairly good. The value of K that gives the best fit for PS was 6.99 GPa, whereas the literature value is 5.36 using the Young's modulus and Poisson's ratio of (3.60 GPa, 0.35). The agreement is fairly good. The value of best fit K for GR was 22.3 GPa, which is comparable but less than the literature value of 36.3 GPa using the Young's modulus and Poisson's ratio of (30.0 GPa, 0.24).

We repeated this procedure for four different cantilevers. Figure 7 shows a comparison between the estimated values and literature values of the effective elasticity for various materials. The straight line corresponds to the case of perfect agreement between the two. The symbols other than circles represent the data by silicon tips, and the circles represent the data by a diamond-coated Si tip. To evaluate Si, only the diamond-coated Si tip was used, because of severe wear of the Si tip.

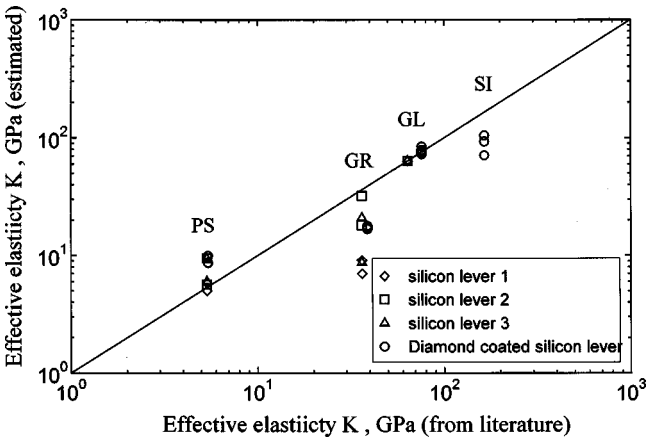

FIG. 7. Comparison between the experimental values of the effective elasticity using the tip shape estimation from the inverse analysis of the resonance frequency and the reported values of the effective elasticity.

We generally obtained a good agreement between the estimated and literature values of the effective elasticity. The agreement for PS was particularly good. The agreement for GR was worse than in PS and the estimated elasticity was usually less than the literature value. A possible reason for this is because we assumed an isotropic indentation mechanics for GR, although GR has a layered structure with a strong anisotropy. A finite-element analysis for the anisotropic contact mechanics would improve the agreement.

Another source of error is noticed in Fig. 3, in which there is some discrepancy between the measured and the estimated force dependence of the resonance frequency for the GR and PS samples. It can be explained by the wear of the tip. Although the tip shape index n had been determined using the data on the GL sample, this value cannot be correct after wear of the tip takes place. In fact, if we treated the tip shape index as an adjustable parameter, and apply an inverse analysis, the tip shape index was estimated to be larger than 5.6 and the agreement in the force dependence was improved.[24]

For some cases, the estimated tip shape index n was more than 10, and the tip shape calculated using the index was significantly more flat than the measured one, as shown in Fig. 6(b). The reason for this error would be (1) the wear of tip changes the tip shape index and (2) the position of the tip apex in contact with the sample is different for different samples.

We verified possibility (1) by a tip profile measurement using a reference tip. However, if we used a diamond-coated tip, we found that the wear resistance of the tip was significantly improved. At the same time, the reproducibility of the estimated effective elasticity was improved. Moreover, we obtained reproducible data for the Si samples, as shown in Fig. 7, which was difficult using the silicon tips. Thus, the wear of the tip is certainly a dominant source of error in the present analysis. Development of a wear resistant tip is clearly one of the most important efforts needed for realizing quantitative AFM when a strong force is acted upon the tip.

Another limitation in the present analysis lies in the necessity of the reference point on the tip profile. Though the reduction of variables by assuming the reference point is useful for a fast convergence of the inverse analysis, measurement of the tip profile using a reference tip needs a certain skill and effort. Moreover, the estimated tip profile may be affected by the selection of the reference point. Therefore, improved analysis without the need for a reference point is required.

ACKNOWLEDGMENT

Part of this work was supported by the Grant-in-Aid for Scientific Research (No. 10450015), and by the Grant-in-Aid for COE Research (No. 11CE2003) from the Ministry of Education, Science, Sports, and Culture of Japan.

[1] G. Binnig, C. F. Quate, and Ch. Gerber, Phys. Rev. Lett. **56**, 930 (1986).
[2] N. Agrait, G. Rubio, and S. Vieira, Phys. Rev. Lett. **74**, 3995 (1995).
[3] M. Radmacher, R. W. Tillman, and H. E. Gaub, Biophys. J. **64**, 735 (1993).
[4] C. Fretigny and C. Basire, J. Appl. Phys. **82**, 43 (1997).
[5] K. Yamanaka and S. Nakano, Jpn. J. Appl. Phys., Part 1 **35**, 93 (1996).
[6] K. Yamanaka and S. Nakano, Appl. Phys. A: Mater. Sci. Process. **66**, S313 (1998).
[7] U. Rabe and W. Arnold, Appl. Phys. Lett. **64**, 1493 (1994).
[8] U. Rabe and W. Arnold, Ann. Phys. **3**, 589 (1994).
[9] U. Rabe, K. Jansen, and W. Arnold, Rev. Sci. Instrum. **67**, 3281 (1996).
[10] O. Wright and N. Nishiguchi, Appl. Phys. Lett. **71**, 626 (1997).
[11] U. Rabe, J. Turner, and W. Arnold, Appl. Phys. A: Mater. Sci. Process. **66**, S277 (1998).
[12] V. Scherer, W. Arnold, and B. Bhushan, Surf. Interface Anal. **27**, 658 (1999).
[13] O. Kolosov and K. Yamanaka, Jpn. J. Appl. Phys., Part 2 **32**, L1095 (1993).
[14] K. Yamanaka, H. Ogiso, and O. Kolosov, Appl. Phys. Lett. **64**, 178 (1994).
[15] K. Yamanaka, H. Ogiso, and O. Kolosov, Jpn. J. Appl. Phys., Part 1 **33**, 3197 (1994).
[16] K. Yamanaka, Thin Solid Films **273**, 116 (1996).
[17] O. Kolosov, M. R. Castell, C. D. Marsh, and G. A. D. Briggs, Phys. Rev. Lett. **81**, 1046 (1998).
[18] S. P. Timoshenko and J. N. Goodier, *Theory of Elasticity* (McGraw-Hill, London, 1970).
[19] C. F. Quate, A. Atalar, and H. K. Wickramasinghe, Proc. IEEE **67**, 1092 (1979).
[20] J. Kushibiki and N. Chubachi, IEEE Trans. Sonics Ultrason. **SU-32**, 189 (1985).
[21] D. Maugis and M. Barquins, J. Phys. D **16**, 1843 (1983).
[22] R. W. Carpick, N. Agrait, D. F. Ogletree, and M. Salmeron, J. Vac. Sci. Technol. B **14**, 1289 (1996).
[23] J. A. Nelder and R. Mead, Comput. J. (UK) **7**, 308 (1965).
[24] K. Yamanaka, A. Noguchi, T. Tsuji, T. Koike, and T. Goto, Surf. Interface Anal. **27**, 600 (1999).
[25] M. Kempf, M. Goken, and H. Vehoff, Appl. Phys. A: Mater. Sci. Process. **66**, S843 (1998).
[26] M. J. P. Musgrave, *Crystal Acoustics* (Holden-Day, San Francisco, CA, 1970), p. 179.
[27] *Handbook of Physical Quantities* (Chemical Rubber, Boca Raton, FL), p. 106.